Journal of Current Science and Technology, October-December 2025 Vol. 15 No. 4, Article 134

ISSN 2630-0656 (Online)

Cite this article: Apisittiwong, T., Yoswathana, N., & Jindal, V. K. (2025). Image-based characterization and statistical optimization of silver nanoparticles biosynthesized using pasteurized milk. *Journal of Current Science and Technology*, *15*(4), Article 134. https://doi.org/10.59796/jcst.V15N4.2025.134

Journal of Current Science and Technology

Journal homepage: https://jcst.rsu.ac.th

Image-Based Characterization and Statistical Optimization of Silver Nanoparticles Biosynthesized Using Pasteurized Milk

Tarit Apisittiwong[1,2,*], Nuttawan Yoswathana[1], and Vinod K Jindal[1]

[1]Department of Chemical Engineering, Faculty of Engineering, Mahidol University, Nakhon Pathom 73170, Thailand
[2]Food Processing Pilot Plant, College of Agricultural Innovation and Food Technology, Rangsit University, PathumThani 12000, Thailand
[2]Faculty of Food Technology, College of Agricultural Innovation and Food Technology, Rangsit University, PathumThani 12000, Thailand

*Corresponding author; E-mail: tarit.a@rsu.ac.th

Received 15 May 2025; Revised 17 June 2025; Accepted 17 June 2025; Published online 20 September 2025

Abstract

Background: Green synthesis of silver nanoparticles (AgNPs) has garnered attention for its sustainability, yet few studies have integrated digital imaging for nanoparticle characterization. Objective: This study aimed to synthesize AgNPs using pasteurized milk as a natural reducing and stabilizing agent, and to optimize synthesis conditions using a rotatable central composite design (CCD), coupled with spectroscopic and image-based analytical methods. Methods: AgNPs were synthesized under varying conditions of milk dilution, $AgNO_3$ concentration, and reaction time. Response variables - SPR wavelength, absorbance, particle size, and imaging-derived parameters (ΔRGB, ΔLab, MGL) were modeled using second-order polynomial regression. Digital imaging under forward, backward, and transmitted light geometries were used to quantify nanoparticle-induced optical changes. Results: Most models showed high predictive power (adjusted $R^2 > 0.80$), with image-based variables (ΔRGB, ΔASM, MGL) strongly correlated with particle concentration and optical density. Optimal conditions (milk:DI 1:15, 2.00 mM $AgNO_3$, 2 h) yielded AgNPs with a strong SPR response (412 nm), small size (95.8 nm), and distinct visual signatures. Predicted responses matched closely with experimental data, validating the model. Conclusion: This study presents a reproducible, low-cost platform for sustainable AgNP synthesis. The incorporation of digital imaging enhances real-time monitoring and offers promising applications in diagnostics, food safety, and green nanotechnology.

Keywords: *silver nanoparticles (AgNPs); green synthesis; pasteurized milk; central composite design (CCD); UV-vis spectroscopy; surface plasmon resonance (SPR); colloidal stability; digital imaging; light scattering*

1. Introduction

Nanotechnology has become a cornerstone of modern science and engineering, offering innovative solutions across sectors such as healthcare, agriculture, environmental protection, and food safety (Thongwattana et al., 2024; Subavathy, et al., 2023). Among the diverse nanomaterials studied, silver nanoparticles (AgNPs) have attracted significant attention due to their potent antimicrobial properties, tunable optical characteristics, and applicability in biosensors and diagnostics (Irwan et al., 2024; Thamilselvi, & Radha, 2017). These qualities make AgNPs ideal candidates for development through sustainable, environmentally friendly synthesis approaches.

The green synthesis of AgNPs, which involves using natural biological substances as reducing and stabilizing agents, offers a safer and more sustainable

alternative to conventional chemical methods. This approach minimizes the need for hazardous chemicals and aligns with green chemistry principles (Simatupang et al., 2021). Various biological matrices, including plant extracts, fungi, and dairy products, have been explored for nanoparticle synthesis (Martin, & Sumayao Jr, 2022; Krishnaraj et al., 2010). Among these, pasteurized milk stands out due to its food-grade nature and rich biochemical composition (Elmegdar et al., 2024). Proteins such as casein and whey, along with bioactive molecules and sugars like lactose, contribute electron-donating functional groups that facilitate the reduction of silver ions (Ag^{+}) to metallic silver (Ag^{0}), while also providing stabilization to prevent nanoparticle agglomeration (Lee et al., 2013; Pandey et al., 2020).

In addition to initiating the reduction of silver ions, milk proteins serve as natural stabilizing agents, forming a stable interface around the nanoparticles due to their abundant functional groups and widespread availability (Suknicom & Borompichai chartkul, 2021). Casein, whey proteins, and other milk constituents contain amino acids and peptide bonds with functional groups such as carboxyl (-COOH), amino (-NH_2), and hydroxyl (-OH) that can bind to the nanoparticle surface (Elmegdar et al., 2024; Changsan et al., 2024). These interactions form a protective layer around the nanoparticles, preventing aggregation and facilitating long-term colloidal stability (Sukmongkolwongs et al., 2024). Such stabilization not only preserves the physicochemical properties of AgNPs but also enhances their uniformity and dispersibility in aqueous media (Maneewattanapinyo et al., 2023), attributes that are particularly advantageous for applications requiring consistent optical behavior and reproducibility in digital imaging analysis (Elumalai, & Navabshan, 2024).

Traditional characterization techniques, such as UV-visible (UV-Vis) spectroscopy and dynamic light scattering (DLS), are widely used to monitor nanoparticle formation and assess size distribution (Dangsaart et al., 2024). UV-Vis spectroscopy, in particular, is crucial for identifying the surface plasmon resonance (SPR) peak, which correlates with particle size, shape, and distribution. However, these techniques often require specialized equipment and may not provide immediate visual feedback. Recent advancements in digital imaging, including light scatter and transmitted light analyses, offer a promising alternative. These methods allow for real-time, non-invasive monitoring of nanoparticle suspensions by capturing changes in color intensity and spatial texture, which are indicative of nanoparticle formation and distribution (Baltasar Sánchez & Gonzalez Sistal, 2014; Fu et al., 2013).

Despite the growing interest in green synthesis, relatively few studies have incorporated image-based techniques for detailed characterization and optimization of biosynthesized AgNPs. Moreover, the combination of digital imaging metrics with statistical modeling approaches, such as response surface methodology, remains underutilized. Integrating these tools could significantly enhance our ability to predict and control nanoparticle synthesis outcomes, particularly under variable experimental conditions.

In this study, we employed a rotatable central composite design (CCD) to systematically investigate the influence of three synthesis parameters: milk dilution ratio, silver nitrate ($AgNO_3$) concentration, and reaction time. Use of CCD allowed for the development of predictive second-order polynomial regression models to evaluate multiple response variables. These included the SPR wavelength, peak UV-Vis absorbance, particle size (via DLS), and a suite of image-based parameters—ΔRGB, ΔLab, and Mean Gray Level (MGL)—captured through forward scatter, backward scatter, and transmitted light analyses. Model adequacy was assessed through statistical metrics such as the coefficient of determination (R^2), adjusted R^2, and standard error of estimate. The goal was not only to optimize synthesis conditions for effective AgNP production but also to demonstrate the feasibility of image-based analysis as a complementary, rapid characterization tool.

2. Objectives

This study aimed to investigate and optimize the green synthesis of silver nanoparticles (AgNPs) using pasteurized milk as a natural reducing and stabilizing agent. A rotatable central composite design (CCD) was employed to examine the effects of milk dilution, $AgNO_3$ concentration, and reaction time on nanoparticle characteristics. AgNPs were characterized using UV-visible spectroscopy, dynamic light scattering (DLS), and digital imaging techniques to evaluate surface plasmon resonance (SPR), particle size, and image-based parameters (ΔRGB, ΔLab, MGL). Predictive second-order polynomial models were developed to assess synthesis efficiency and identify optimal conditions for potential applications in food safety and spoilage detection.

3. Materials and Methods

3.1 Materials

Commercial pasteurized milk was procured from a local supermarket in Thailand and used without further treatment. Silver nitrate ($AgNO_3$, analytical grade, ≥ 99% purity) was supplied by Merck (Germany). All dilutions and preparations were performed using deionized (DI) water. Glassware and cuvettes were sterilized and rinsed thoroughly with DI water prior to use to eliminate contamination.

3.2 Biosynthesis of Silver Nanoparticles

Silver nanoparticles (AgNPs) were synthesized using a green, one-step process by reacting pasteurized milk with $AgNO_3$. All experiments were carried out with continuous stirring at 120 rpm under 72 W LED white daylight exposure at room temperature (28 ± 2°C).

Experimental runs were performed following a rotatable central composite design (CCD), in which varying proportions of milk and $AgNO_3$ were mixed and allowed to react for predetermined durations. No external heating or pH adjustment was applied. A visible color change from milky white to pale yellow or brown indicated the formation of AgNPs via the reduction of Ag^+ ions by milk proteins and bioactive compounds.

3.3 Experimental Design and Optimization

The biosynthesis process was systematically optimized using a rotatable central composite design (CCD) to investigate the effects of three independent variables on silver nanoparticle formation: milk dilution ratio (X_1), silver nitrate ($AgNO_3$) concentration (X_2), and reaction time (X_3). The experimental matrix consisted of 20 runs, including factorial, axial, and center points, enabling the exploration of both linear and quadratic effects and interactions among variables.

Each factor was tested at five coded levels (−α, −1, 0, +1, +α), as shown in Table 1, which provides the corresponding actual values for each coded level.

The table presents the coded and actual experimental levels of three synthesis parameters: milk to deionized water dilution ratio (X_1), silver nitrate ($AgNO_3$) concentration (X_2), and reaction time (X_3). These values were used to construct a CCD matrix for model development and multi-response optimization. This design allowed for the development of second-order polynomial regression models capable of accurately predicting the influence of synthesis parameters on multiple nanoparticle properties.

The response variables included SPR wavelength (Y_1), UV-vis absorbance (Y_2), particle size (Y_3), forward and backward scatter intensities, and GLCM-based texture metrics (Y_4–Y_{10}), and transmitted light colorimetric and brightness parameters (Y_{11}–Y_{14}). Multi-response optimization was performed using the Solver function in Microsoft Excel to identify synthesis conditions that maximize or minimize each target response.

3.4 Characterization Techniques

3.4.1 UV-Visible Spectroscopy

Surface plasmon resonance (SPR) and absorbance peaks were analyzed using a UV-visible spectrophotometer (UV-1800, SHIMADZU, Japan) across a wavelength range of 300–700 nm. Measurements were performed using 1 cm quartz cuvettes at room temperature.

3.4.2 Dynamic Light Scattering (DLS)

Hydrodynamic particle size distributions were determined using a Nano-ZS Nanoparticle Analyzer (Zen3600, Malvern, U.K.). To minimize interference from milk components during DLS measurements, the samples were diluted prior to analysis. Measurements were carried out on colloidal suspensions with a dilution factor of 10, reducing the contribution of larger milk particles and background scattering, and allowing for more accurate characterization of the AgNPs in suspension.

Table 1 Coded levels and actual values of independent variables used in the rotatable central composite design (CCD) for biosynthesis of silver nanoparticles

Independent Variables	Codes	Actual values for variables				
		axial point	factorial point	center points	factorial point	axial point
		z = -1.682	z = -1	z = 0	z = 1	z =1.682
Milk: DI water ratio (v/v)	X1	1:6.6	1:10	1:15	1:20	1:23.4
$AgNO_3$ concentration (mM)	X2	0.66	1	1.5	2	2.25
Time (h)	X3	0.32	1	2	3	3.68

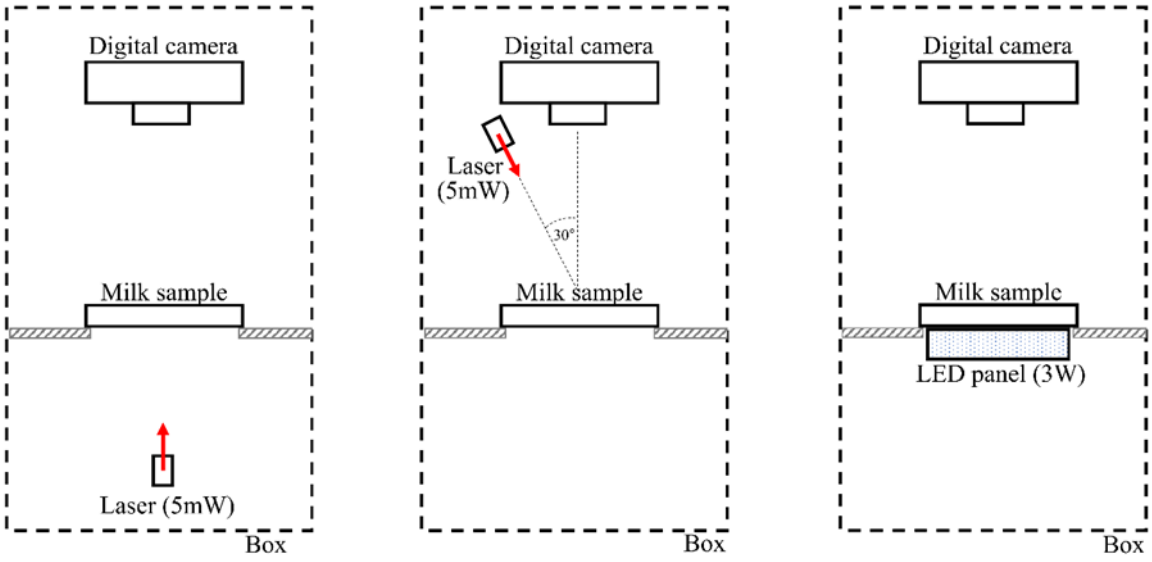

Figure 1 Schematic (a) Forward Scatter (b) Backward Scatter (c) Transmitted Light

3.4.3 Digital Imaging and Light Scatter Analysis

Measurements were conducted inside a closed box to prevent interference from external light. Twenty milliliters of AgNP suspension were placed in a Petri dish, as shown in the schematic diagram (Figure 1). Images were captured immediately after each synthesis using a digital camera (Canon Kiss X7) and analyzed using ImageJ software based on three geometric parameters:

- Forward Scatter: To capture scattering from small particles and aggregates.
- Backward Scatter: To minimize multiple scattering effects and highlight concentration gradients.
- Transmitted Light: To evaluate colorimetric changes and grayscale distribution.

From these images, various parameters were extracted, including:

- Color difference metrics: ΔRGB, ΔLab
- Texture metrics: ΔAngular Second Moment (ΔASM), ΔContrast, ΔCorrelation, ΔInverse Difference Moment (ΔIDM)
- Brightness measures: Mean Gray Level (MGL), and MGL Weighted

3.5 Statistical Modeling and Data Analysis

Second-order polynomial regression models were developed for fourteen response variables (Y_1–Y_{14}) using the CCD-based experimental dataset. These models evaluated the effects of milk dilution (X_1), $AgNO_3$ concentration (X_2), and reaction time (X_3) on nanoparticle characteristics. The general form of the regression equation used is as follows:

$$Y = \beta_0 + \sum_{i=1}^{3}\beta_i . X_i + \sum_{i=1}^{3}\beta_{ii} . X_i^2 + \sum_{i=1}^{2}\sum_{j=i+1}^{3}\beta_{ij} . X_i . X_j \quad (1)$$

where Y represents the response variable; β_0 is the constant term; β_i, β_{ii}, and β_{ij} denote the coefficients for linear, quadratic, and interaction effects, respectively; and X_i and X_j represent the independent variables. Model parameters were estimated using Microsoft Excel, and optimization was conducted with the Solver add-in. Model quality was assessed using the coefficient of determination (R^2), adjusted R^2, standard error, and ANOVA at a 95% confidence level ($p < 0.05$). Residual plots and lack-of-fit tests were also used to validate model adequacy.

4. Results and Discussion

4.1 Biosynthesis of AgNPs Using Pasteurized Milk

The successful biosynthesis of silver nanoparticles (AgNPs) using pasteurized milk was initially confirmed by a distinct visual transformation in the reaction mixture. Upon combining milk with $AgNO_3$ and incubating under various conditions defined by the CCD matrix, the color of the solution shifted from its original milky white to shades ranging from pale yellow to dark brown. This color change, visible to the naked eye, is characteristic of nanoparticle formation and is attributed to the excitation of surface plasmon resonance (SPR) in AgNPs.

This transformation indicates the reduction of Ag^+ ions to metallic silver (Ag^0) by milk constituents, particularly proteins such as casein and whey. These proteins not only facilitate electron transfer but also act as capping agents, stabilizing the nanoparticles and preventing their aggregation. The degree of color intensity was qualitatively observed to vary with different synthesis conditions, suggesting that the milk dilution ratio, $AgNO_3$ concentration, and reaction time influence nanoparticle nucleation and growth.

The reaction was reproducible under ambient conditions (28 ± 2°C) without the need for additional chemical reducers, external heating, or pH adjustment. This simplicity underscores the viability of pasteurized milk as a sustainable and practical medium for green synthesis. Furthermore, the use of commercially available milk enhances the approach's scalability and relevance for real-world applications.

Figure 2 illustrates a representative example of the color change during synthesis, with (a) showing the initial milk solution and (b) displaying the resulting brown-colored colloidal suspension indicative of AgNP formation. This visual evidence laid the groundwork for detailed spectroscopic, size, and image-based analyses, which are discussed in the following sections.

4.2 AgNP Characterization: UV-Visible Spectroscopy and DLS Analysis

4.2.1 UV-Visible Spectroscopy

UV-visible spectroscopy was used as a primary tool to confirm the formation and evaluate the optical properties of biosynthesized AgNPs. Figure 3 presents representative UV-visible spectra from selected runs, highlighting how variations in synthesis conditions influence SPR behavior and, consequently, nanoparticle characteristics. The experimental conditions corresponding to each graph are detailed in Table 2. All samples exhibited distinct surface plasmon resonance (SPR) bands in the range of 380–465 nm, a signature feature of colloidal silver nanoparticles. The exact position and intensity of the SPR peak varied depending on the synthesis conditions, reflecting differences in particle size, shape, and concentration.

(a) (b)

Figure 2 Visual confirmation of silver nanoparticle (AgNP) formation using pasteurized milk. (a) Initial reaction mixture consisting of pasteurized milk and $AgNO_3$, showing a milky white appearance. (b) Resulting colloidal suspension of sample 1 (X_1 = 1:10 v/v, X_2 = 1 mM, X_3 = 1 h) displayed a light brown color after incubation, indicating the successful reduction of Ag^+ to Ag^0 and AgNP formation via surface plasmon resonance (SPR)

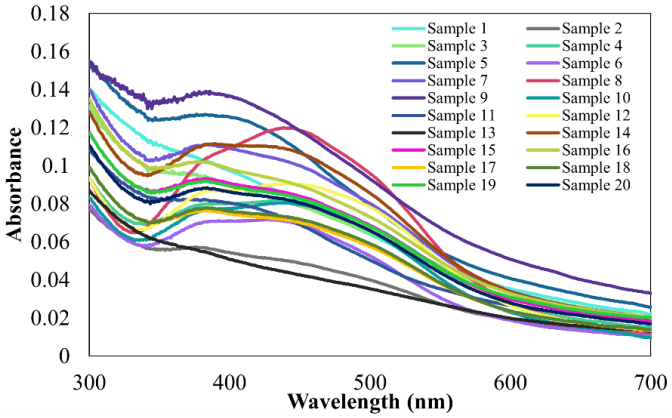

Figure 3 UV-visible absorption spectra of silver nanoparticles (AgNPs) synthesized under varying experimental conditions defined by the CCD matrix, using a dilution factor of 50.

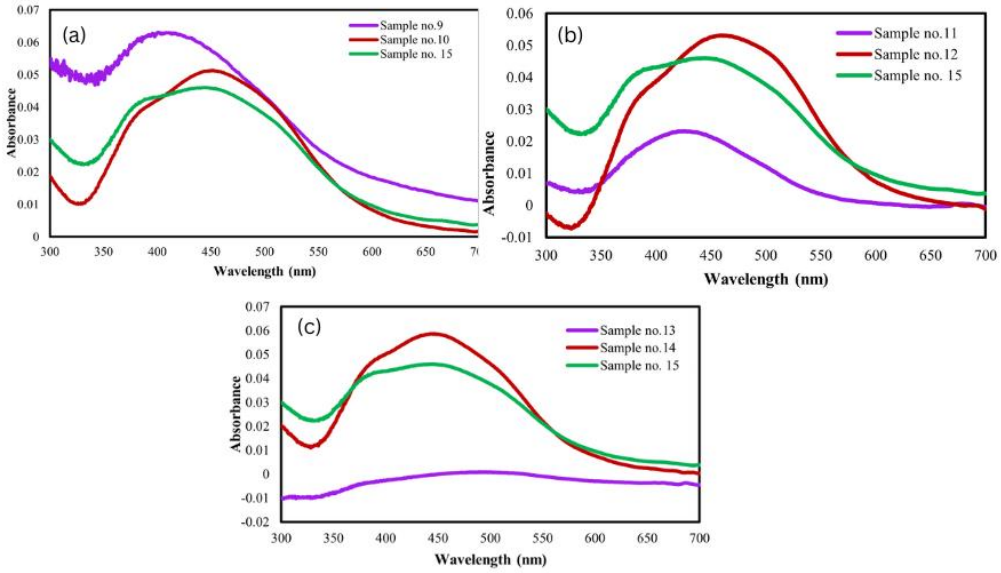

Figure 4 Effect of individual synthesis parameters on UV-visible absorbance spectra of AgNP suspensions. (a) Influence of milk dilution ratio (samples 9, 10, 15); (b) Effect of $AgNO_3$ concentration (samples 11, 12, 15); (c) Variation with reaction time (samples 13, 14, 15)

High absorbance values typically indicate greater nanoparticle yield and dispersion uniformity. For instance, samples such as Runs 8, 9, and 12 showed strong absorbance peaks (>2.5), suggesting efficient nanoparticle formation under those specific parameter combinations. Conversely, broader or red-shifted peaks, observed in samples like Runs 2 and 13—are commonly associated with larger or more polydisperse particles (Kelly et al., 2003; Rechberger et al., 2003).

A blue shift in the SPR peak (i.e., movement toward shorter wavelengths) generally corresponds to the presence of smaller, spherical particles, while red shifts indicate either larger particles or the onset of agglomeration. These spectral variations are consistent with the experimental variables defined by the CCD, particularly where higher $AgNO_3$ concentrations and longer reaction times favored the formation of smaller, more uniform particles (Asif et al., 2022; Krishnaraj et al., 2010; Dubey et al., 2010). In all experiments, UV-vis absorption curves were collected after diluting the milk samples with a dilution factor of 50 to reduce turbidity and performing baseline correction. In some cases, samples were also filtered prior to measurement to remove larger scattering particles. These steps minimized scattering effects and allowed accurate determination of absorption features.

4.2.2 Dynamic Light Scattering (DLS) Analysis

Dynamic light scattering (DLS) analysis was used to determine the hydrodynamic size distribution of silver nanoparticles (AgNPs) synthesized under different experimental conditions. Particle sizes varied significantly across the CCD matrix, ranging from 90.75 nm to 159.97 nm, confirming the formation of nanoparticles within the colloidal scale under all tested synthesis conditions. Although TEM imaging was not performed in this study, the AgNP size was estimated based on DLS, which is consistent with previously reported characteristics of silver nanoparticles in similar systems (Simatupang et al., 2021).

The smallest particle size was observed in Run 12 (90.75 nm), which used a milk dilution ratio of 1:15, a high $AgNO_3$ concentration of 2.25 mM, and a reaction time of 2 hours. These conditions likely promoted rapid nucleation while limiting secondary growth, leading to more uniform and well-dispersed nanoparticles. Conversely, the largest particle size was recorded in Run 3 (159.97 nm), where lower milk dilution and a longer reaction time may have favored particle aggregation or growth into larger clusters. The dilution ratio of milk plays a critical role in both the observed size and optical properties of AgNPs, primarily due to the complex matrix of milk, which includes proteins, lipids, and other light-scattering

components. As demonstrated by Li et al. (2022), this complex matrix can interfere with nanoparticle size measurements unless the samples are effectively diluted or enzymatically digested.

The size distribution results were consistent with trends observed in the UV-visible spectroscopy data. Samples that exhibited smaller particle sizes typically corresponded with blue-shifted SPR peaks and higher absorbance values, suggesting stronger nanoparticle formation and better colloidal stability. For instance, Run 8 also demonstrated a small particle size along with high optical absorbance, highlighting its synthesis efficiency.

These findings support the importance of synthesis parameters—especially $AgNO_3$ concentration and reaction time—in controlling nanoparticle size. An optimal parameter range appears to lie within a milk:DI water ratio of 1:15 to 1:20, $AgNO_3$ concentration between 1.5 to 2.25 mM, and reaction times around 2 hours.

Overall, the optical and stability characteristics of the synthesized AgNPs were strongly influenced by the synthesis parameters, namely, milk and DI water ratio, $AgNO_3$ concentration and reaction time. These factors affected the surface plasmon resonance (SPR) behavior observed in UV-Vis spectroscopy reflecting changes in particle size and distribution and were further supported by DLS measurements, which confirmed good colloidal stability under optimized conditions.

4.3 Light Scattering and Image-Based Analysis

To complement traditional spectroscopic and particle size analyses, digital imaging techniques were employed to capture the visual and spatial characteristics of AgNP suspensions. These techniques provided a rapid, non-invasive means of monitoring nanoparticle synthesis through variations in light scattering, color intensity, and image texture. Three configurations were used—forward scatter, backward scatter, and transmitted light imaging—to extract quantitative parameters related to particle dispersion, optical density, and colloidal uniformity.

Table 2 Coded and actual levels of synthesis variables (milk dilution, $AgNO_3$ concentration, and reaction time) and corresponding response values (SPR wavelength, UV-vis absorbance, and particle size) for each experimental run based on the central composite design (CCD)

Designed code	Sample	Variables			Results		
		Milk:DI water dilution ratios (v/v ratio) X_1	$AgNO_3$ conc. (mM) X_2	Time (h) X_3	SPR wavelength (nm) Y_1	Absorbance Y_2	Size by number (nm) Y_3
8 Factorial experiment (Code value -1 and +1)	1	1:10	1	1	427.5	0.94	154.22
	2	1:20	1	1	465	0.57	118.42
	3	1:10	2	1	463.5	1.08	159.97
	4	1:20	2	1	450	2.62	113.59
	5	1:10	1	3	414	3.14	159.58
	6	1:20	1	3	438	2.10	103.19
	7	1:10	2	3	450	1.90	113.40
	8	1:20	2	3	447	4.44	91.22
6 Axial (Code value -1.682 and +1.682)	9	1:6.6	1.5	2	408.5	3.15	146.30
	10	1: 23.4	1.5	2	451.5	2.57	106.29
	11	1:15	0.66	2	424.5	1.16	125.55
	12	1:15	2.25	2	462	2.66	90.75
	13	1:15	1.5	0.32	491	0.05	122.55
	14	1:15	1.5	3.68	446.5	2.94	114.48
6 Central (Code value 0)	15	1:15	1.5	2	445	2.30	107.88
	16	1:15	1.5	2	446	2.28	113.08
	17	1:15	1.5	2	445.5	2.56	106.38
	18	1:15	1.5	2	450.5	1.62	99.96
	19	1:15	1.5	2	445.25	2.20	113.99
	20	1:15	1.5	2	449	1.68	111.82

4.3.1 Forward Scattered Light Analysis

Forward scatter light intensity (Y_4) was used to assess the distribution and concentration of nanoparticles. Across all experimental runs, forward scatter intensity values ranged from 6.49 to 15.84. Higher intensities generally indicated greater particle concentrations or smaller, more uniform particles due to enhanced Mie scattering.

Texture features derived from Gray Level Co-occurrence Matrix (GLCM) analysis—including angular second moment (ΔASM, Y_5), contrast (ΔContrast, Y_6), and correlation (ΔCorrelation, Y_7)—provided additional insights. For example, higher forward scatter intensity was associated with lower ΔASM values, indicating smoother and more homogeneous textures. Runs 11 and 13, which had high forward intensity, exhibited minimal ΔASM, suggesting dense and uniform nanoparticle distribution. In contrast, Run 8 showed the lowest intensity and highest ΔASM, indicating a more heterogeneous system.

4.3.2 Backward Scattered Light Analysis

Backward scatter measurements helped evaluate particle behavior in more concentrated or aggregated states by minimizing multiple scattering. Intensity values (Y_8) ranged from 7.04 to 19.19, with higher values again pointing to denser colloidal suspensions. Similar to forward scatter analysis, backward ΔASM (Y_9) and inverse difference moment (ΔIDM, Y_{10}) values showed inverse relationships with intensity. Low ΔASM and ΔIDM values suggested well-packed, optically consistent nanoparticle populations. Run 13 displayed the highest backward intensity with minimal texture variation, reinforcing its status as a condition yielding dense and compact AgNP distributions.

4.3.3 Transmitted Light and Colorimetric Analysis

Transmitted light analysis provided additional insights into the optical characteristics of AgNP suspensions through four image-based parameters: RGB color difference (ΔRGB, Y_{11}), Lab color difference (ΔLab, Y_{12}), mean gray level (MGL, Y_{13}), and MGL Weighted (Y_{14}). Samples with high ΔRGB and ΔLab values corresponded to darker, more optically dense suspensions—indicating greater nanoparticle concentration and stronger light absorption.

An inverse relationship was consistently observed between colorimetric contrast (ΔRGB, ΔLab) and grayscale brightness (MGL). For instance, Run 8 exhibited the highest ΔRGB (391.67) and the lowest MGL (33.54), reflecting a dense, dark suspension, while Run 13 showed the lowest ΔRGB (190.36) and the highest MGL (157.54), indicating a lighter, less concentrated colloid.

These observations confirm a strong inverse relationship between color intensity and gray level metrics: darker, more optically dense samples had higher colorimetric differences but lower brightness levels. This relationship validates transmitted light analysis as a reliable surrogate for estimating nanoparticle concentration and synthesis efficacy. A comprehensive summary of the image-based response variables derived from forward/backward scatter and transmitted light analysis is presented in Tables 3 and 4.

Figure 5 visually illustrates this trend, presenting representative AgNP suspensions with increasing MGL values from images (a) to (e). The progression from dark brown to pale yellow correlates with reduced nanoparticle density and optical absorbance. This confirms MGL as a practical surrogate for estimating AgNP concentration and optical activity, supporting its use in non-invasive, real-time process monitoring.

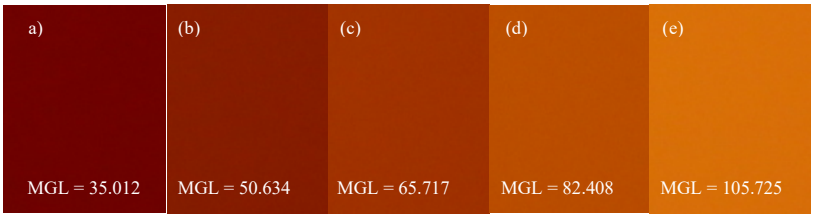

Figure 5 Visual representation of silver nanoparticle (AgNP) suspensions with varying Mean Gray Level (MGL) values under transmitted light imaging. Images (a) to (e) show progressively increasing MGL values (from 35.012 to 105.725), corresponding to a visual shift from dark brown to pale yellow.

Table 3 Forward and backward light scattering parameters derived from digital imaging analysis of AgNP suspensions synthesized under different experimental conditions. Parameters include forward and backward scatter intensity, and GLCM-based texture metrics: angular second moment difference (ΔASM), contrast difference (ΔContrast), correlation difference (ΔCorrelation), and inverse difference moment change (ΔIDM), providing insights into nanoparticle dispersion and optical behavior

Run no.	Forward scatter light				Backward scatter light		
	Intensity (Y_4)	ΔASM (Y_5)	ΔContrast (Y_6)	ΔCorrelation (Y_7)	Intensity (Y_8)	ΔASM (Y_9)	ΔIDM (Y_{10})
1	12.68	0.0095	-0.1488	0.0005	18.51	0.0068	0.0440
2	15.27	0.0088	-0.2038	0.0000	16.10	0.0065	0.0472
3	9.13	0.0213	-0.1850	0.0020	15.07	0.0145	0.0562
4	9.35	0.0273	-0.2573	0.0010	9.93	0.0278	0.0833
5	10.91	0.0150	-0.1643	0.0010	16.93	0.0095	0.0495
6	13.37	0.0130	-0.2438	0.0000	13.80	0.0140	0.0838
7	8.13	0.0265	-0.1995	0.0020	13.45	0.0220	0.0705
8	6.52	0.0418	-0.2493	0.0020	7.04	0.0410	0.0828
9	9.47	0.0185	-0.1945	0.0020	15.38	0.0175	0.0508
10	9.76	0.0283	-0.2833	0.0000	9.24	0.0280	0.0748
11	15.35	0.0068	-0.1470	0.0005	18.31	0.0055	0.0500
12	6.49	0.0385	-0.2148	0.0030	9.31	0.0330	0.0692
13	15.84	0.0048	-0.0915	0.0000	19.19	0.0040	0.0305
14	9.57	0.0230	-0.1858	0.0015	12.23	0.0203	0.0643
15	11.17	0.0173	-0.2135	0.0010	14.10	0.0133	0.0607
16	11.32	0.0173	-0.2198	0.0010	14.41	0.0130	0.0595
17	10.66	0.0210	-0.2428	0.0010	13.15	0.0170	0.0803
18	11.15	0.0168	-0.1793	0.0010	13.80	0.0145	0.0665
19	11.57	0.0160	-0.2188	0.0010	14.39	0.0130	0.0717
20	11.19	0.0180	-0.1773	0.0010	13.80	0.0150	0.0612

Table 4 Transmitted light colorimetric and grayscale parameters of AgNP suspensions derived from digital image analysis. Color metrics include RGB color difference (ΔRGB) and Lab color difference (ΔLab), while brightness measures include Mean Gray Level (MGL) and MGL Weighted. These values reflect variations in nanoparticle concentration and optical density across the experimental runs

Run no.	Δ RGB (Y_{11})	Δ Lab (Y_{12})	MGL (Y_{13})	MGL weighted (Y_{14})
1	279.12	82.63	113.23	132.83
2	255.17	80.25	132.80	153.42
3	343.76	88.07	61.37	68.45
4	366.13	92.44	50.17	52.64
5	315.59	87.48	85.01	97.45
6	308.98	89.74	97.39	112.47
7	368.56	91.73	44.45	45.94
8	391.67	95.17	33.54	30.22
9	350.86	88.95	49.46	53.43
10	352.47	92.15	60.82	65.52
11	276.01	84.67	126.78	154.25
12	387.09	94.75	35.83	33.29
13	190.36	55.24	157.54	170.24
14	362.38	92.80	52.54	55.10
15	339.56	90.86	69.52	76.93
16	335.85	90.49	72.43	80.70
17	341.94	90.24	67.17	74.49
18	334.46	90.71	73.76	82.18
19	333.56	90.75	74.56	83.11
20	340.80	91.02	68.58	75.67

4.4 Regression Model Validation and Statistical Significance

To quantitatively analyze the effects of synthesis variables on silver nanoparticle (AgNP) characteristics, second-order polynomial regression models (Equation 1) were developed using the response surface methodology (RSM) framework. Each model predicted one of the 14 response variables—ranging from spectroscopic and particle size metrics to image-based texture and color parameters—based on three independent factors: milk dilution ratio (X_1), $AgNO_3$ concentration (X_2), and reaction time (X_3).

Model performance was evaluated using the coefficient of determination (R^2), adjusted R^2, and standard error of estimate. Most models showed strong predictive capability, with adjusted R^2 values exceeding 0.80 for key responses such as SPR wavelength (Y_1), peak absorbance (Y_2), particle size (Y_3), and image-based metrics like forward/backward scatter intensity (Y_4, Y_8) and ΔASM (Y_5, Y_9). These values indicate that the regression models effectively captured the underlying synthesis dynamics.

However, two response variables, ΔIDM (Y_{10}) and ΔLab (Y_{12}), exhibited comparatively lower adjusted R^2 values (below 0.80), suggesting limited model accuracy for these outputs. This may be due to higher image variability, unmodeled environmental factors (e.g., lighting, background noise), or intrinsic complexity in quantifying these parameters. As such, ΔIDM and ΔLab should be interpreted with caution and ideally verified through confirmation experiments or supported by complementary techniques (e.g., hyperspectral imaging or colorimetric calibration curves), particularly when used for diagnostic or sensor development purposes.

The complete set of regression equations, statistical coefficients, and model performance summaries are presented in Table 5. These models form the analytical foundation for optimization discussed in the following section.

4.5 Optimization of Synthesis Conditions

The synthesis was optimized using a central composite design (CCD), which systematically explored the effects of milk dilution ratio, silver nitrate concentration, and reaction time. A multi-response regression approach was applied to identify the optimal combination of parameters that produced stable, well-dispersed AgNPs with desirable optical properties. Optimization was guided by statistical modeling and supported by spectroscopic and visual indicators of nanoparticle quality.

Characterization techniques included UV-Vis spectroscopy to monitor surface plasmon resonance (SPR), providing insight into particle size, concentration, and aggregation, and dynamic light scattering (DLS) to assess hydrodynamic diameter and dispersion stability. Importantly, digital imaging was integrated as a real-time quality assessment tool. A controlled imaging setup was used to capture reaction progress under different lighting conditions. Image analysis was performed using software to extract parameters such as color contrast, brightness, and texture features, which served as proxies for nanoparticle concentration, size uniformity, and aggregation state.

The Solver tool in Microsoft Excel was employed for desirability-based optimization, incorporating user-defined criteria to balance conflicting responses. Specifically, the optimization targeted:

- **Minimization** of particle size (Y_3) and brightness metrics (MGL, MGL Weighted: Y_{13}, Y_{14}),
- **Maximization** of SPR absorbance (Y_2), color contrast (ΔRGB and ΔLab: Y_{11}, Y_{12}), and texture uniformity (ΔASM and ΔIDM: Y_5, Y_{10}),
- **Stabilization** of SPR wavelength (Y_1) and scatter intensities (Y_4, Y_8) within ideal mid-range values.

The optimal combination was determined to be:

- **Milk dilution ratio:** 1:15 (v/v),
- **$AgNO_3$ concentration:** 2.00 mM,
- **Reaction time:** 2.0 hours.

Under these conditions, the model predicted a strong SPR response at approximately 410 nm, high absorbance (>2.4), particle size below 100 nm, and favorable image-based responses (ΔRGB ≈ 370, MGL ≈ 40). These results were consistent with experimental data from Run 12, which closely matched the optimal parameters.

Table 6 presents the predicted and observed values for all key responses under optimized conditions, confirming the model's validity and practical applicability. This multi-criteria optimization approach demonstrates the value of integrating statistical modeling with visual and spectroscopic analyses to guide green nanoparticle synthesis with precision.

Table 5 Second-order polynomial regression equations, model coefficients, and performance metrics (R^2, adjusted R^2, and standard error of estimate) for 14 response variables in the CCD-based biosynthesis of silver nanoparticles (AgNPs)

Response variables	Model	R^2	Adjusted R^2	Standard Error
SPR wavelength (nm)	$Y_1 = 446.9710 + 8.5901\ X_1 + 9.4503\ X_2 - 9.6534\ X_3 - 9.7500\ X_1X_2 - 0.3750\ X_1X_3 + 3.0000\ X_2X_3 - 6.5946\ X_1^2 - 1.9112\ X_2^2 + 7.1022\ X_3^2$……(2)	0.9294	0.8658	6.6934
Peak Absorbance	$Y_2 = 2.1050 + 0.1239\ X_1 + 0.4230\ X_2 + 0.8221\ X_3 + 0.6859\ X_1X_2 + 0.0409\ X_1X_3 – 0.1366\ X_2X_3 + 0.2695\ X_1^2 – 0.0667\ X_2^2 – 0.2147X_3^2$…… (3)	0.9027	0.8151	0.4379
Size by number (nm)	$Y_3 = 108.5765 - 16.6965\ X_1 - 8.4754\ X_2 - 6.7615\ X_3 + 2.9536\ X_1X_2 + 0.4503\ X_1X_3 - 7.3849\ X_2X_3 + 7.9618\ X_1^2 + 1.5483\ X_2^2 + 5.2117\ X_3^2$ ……(4)	0.8702	0.7534	10.3064
Intensity	$Y_4 = 11.1885 + 0.3042\ X_1 - 2.4895\ X_2 - 1.3202\ X_3 - 0.8056\ X_1X_2 - 0.2455\ X_1X_3 - 0.0200\ X_2X_3 - 0.6370\ X_1^2 - 0.1755\ X_2^2 + 0.4565\ X_3^2$ ……(5)	0.9630	0.9296	0.6949
ΔASM	$Y_5 = 0.0177 + 0.0026\ X_1 + 0.0091\ X_2 + 0.0044\ X_3 + 0.0030\ X_1X_2 + 0.0010\ X_1X_3 + 0.0013\ X_2X_3 + 0.0021\ X_1^2 + 0.0018\ X_2^2 - 0.0013\ X_3^2$ ……(6)	0.9762	0.9548	0.0020
ΔContrast	$Y_6 = - 0.2078 - 0.0297\ X_1 - 0.0179\ X_2 - 0.0161\ X_3 + 0.0016\ X_1X_2 - 0.0002\ X_1X_3 + 0.0061\ X_2X_3 - 0.0153\ X_1^2 + 0.0052\ X_2^2 + 0.0201\ X_3^2$……(7)	0.8248	0.6671	0.0256
ΔCorrelation	$Y_7 = 0.0010 - 0.0004\ X_1 + 0.0007\ X_2 + 0.0003\ X_3 + 0.0001\ X_1X_2 + 0.0001\ X_1X_3 + 0.0001\ X_2X_3 - 0.00002\ X_1^2 + 0.0002\ X_2^2 - 0.0001\ X_3^2$……(8)	0.9353	0.8770	0.0003
Intensity	$Y_8 = 13.9442 - 2.0083\ X_1 - 2.5607\ X_2 - 1.4713\ X_3 - 0.7515\ X_1X_2 - 0.2473\ X_1X_3 - 0.0797\ X_2X_3 - 0.5959\ X_1^2 - 0.0644\ X_2^2 + 0.6056\ X_3^2$ ……(9)	0.9740	0.9507	0.7133
ΔASM	$Y_9 = 0.0143 + 0.0040\ X_1 + 0.0084\ X_2 + 0.0043\ X_3 + 0.0035\ X_1X_2 + 0.0013\ X_1X_3 + 0.0013\ X_2X_3 + 0.0029\ X_1^2 + 0.0016\ X_2^2 - 0.0009\ X_3^2$ ……(10)	0.9864	0.9742	0.0015
ΔIDM	$Y_{10} = 0.0664 + 0.0086\ X_1 + 0.0074\ X_2 + 0.0082\ X_3 + 0.0002\ X_1X_2 + 0.0020\ X_1X_3 - 0.0035\ X_2X_3 + 0.0004\ X_1^2 - 0.0007\ X_2^2 - 0.0050\ X_3^2$ ……(11)	0.7782*	0.5786	0.0095
Δ RGB	$Y_{11} = 337.3786 + 1.2921\ X_1 + 36.4691\ X_2 + 31.4796\ X_3 + 9.5068\ X_1X_2 + 2.2609\ X_1X_3 - 4.9920\ X_2X_3 + 7.0131\ X_1^2 - 0.0963\ X_2^2 - 19.6012\ X_3^2$ ……..…(12)	0.9025	0.8147	20.6382
Δ Lab	$Y_{12} = 90.5464 + 0.9564\ X_1 + 3.2403\ X_2 + 6.1428\ X_3 + 0.9914\ X_1X_2 + 0.4626\ X_1X_3 - 0.9918\ X_2X_3 + 0.8069\ X_1^2 + 0.5104\ X_2^2 - 5.0352\ X_3^2$…… (13)	0.7840*	0.5896	5.4818
MGL	$Y_{13} = 71.1259 + 2.1213\ X_1 - 28.6920\ X_2 - 20.0454\ X_3 - 6.7570\ X_1X_2 - 0.8636\ X_1X_3 + 3.7600\ X_2X_3 - 6.4133\ X_1^2 + 2.8366\ X_2^2 + 11.2241\ X_3^2$ ……(14)	0.9370	0.8803	11.5992
MGL weighted	$Y_{14} = 78.9266 + 1.7866\ X_1 - 36.7814\ X_2 - 23.0598\ X_3 + -8.3930\ X_1X_2 - 0.6849\ X_1X_3 + 3.9250\ X_2X_3 - 7.3847\ X_1^2 + 4.7381X_2^2 + 11.4174X_3^2$……..…(15)	0.9570	0.9183	11.5474

Values marked with an asterisk (*) indicate adjusted $R^2 < 0.80$ and should be interpreted with caution. Confirmation experiments or supplementary validation are recommended for these models

Table 6 Predicted versus experimental values of key response variables for the optimized silver nanoparticle (AgNP) synthesis conditions.

Response Variable	Predicted Value	Experimental Value	Absolute Error
SPR Wavelength (nm)	410	412	2
Absorbance (a.u.)	2.45	2.51	0.06
Particle Size (nm)	98.7	95.8	2.9
ΔRGB	370.2	368	2.2
ΔLab	85.6	82.3	3.3
Mean Gray Level (MGL)	40.1	41.6	1.5
MGL Weighted	38.9	40.5	1.6
ΔASM (Fwd)	0.012	0.014	0.002
ΔContrast (Fwd)	6.73	6.85	0.12
ΔIDM (Bwd)	0.032	0.031	0.001

Note:
1) The optimal conditions were identified as milk dilution ratio 1:15 (v/v), $AgNO_3$ concentration 2.00 mM, and reaction time 2 hours
2) Optimization was based on multi-response desirability analysis using regression models for SPR wavelength, absorbance, particle size, and image-based metrics

5. Conclusion

This study successfully demonstrated the green synthesis and multi-response optimization of silver nanoparticles (AgNPs) using pasteurized milk as a natural reducing and stabilizing agent. The integration of a rotatable central composite design (CCD) with digital imaging and conventional analytical techniques (UV-Vis spectroscopy and DLS) enabled a comprehensive evaluation of synthesis conditions and their impact on nanoparticle characteristics.

The predictive models developed for fourteen response variables, including SPR wavelength, particle size, absorbance, and a suite of image-based parameters, showed strong statistical significance, with most models achieving adjusted R^2 values above 0.80. Notably, the image-derived metrics such as ΔRGB, ΔASM, and MGL proved to be effective non-invasive indicators for monitoring colloidal AgNP formation.

The optimal synthesis conditions were identified as a milk dilution ratio of 1:15 (v/v), $AgNO_3$ concentration of 2.00 mM, and a reaction time of 2.0 hours. Under these conditions, the experimentally obtained nanoparticle properties closely matched the model predictions, validating the accuracy and applicability of the regression approach. While most responses were modeled with high reliability, parameters such as ΔIDM and ΔLab should be interpreted with caution and verified through further confirmation, as their models exhibited lower adjusted R^2 values.

Overall, this work provides a robust and reproducible method for sustainable AgNP synthesis and introduces a novel image-based framework for characterizing and optimizing nanomaterial systems. The approach holds promise for broader applications in food safety diagnostics, antimicrobial materials, and real-time quality monitoring in green nanotechnology.

6. Acknowledgements

The authors would like to express their appreciation to the Integrated Chemical Engineering Program, Department of Chemical Engineering, Faculty of Engineering, Mahidol University, Salaya Campus, for providing facility support. We also extend our sincere appreciation to our colleagues at the Food Processing Pilot Plant and Faculty of Food Technology, Rangsit University, for their support.

7. CrediT Statement

Tarit Apisittiwong: Investigation, Validation, Formal analysis, Writing – original draft.
Nuttawan Yoswathana: Validation, Resources, Funding acquisition.
Vinod K Jindal: Conceptualization, Methodology, Supervision, Writing – review & editing

8. References

Asif, M., Yasmin, R., Asif, R., Ambreen, A., Mustafa, M., & Umbreen, S. (2022). Green synthesis of silver nanoparticles (AgNPs), structural characterization, and their antibacterial potential. *Dose-response*, *20*(2). https://doi.org/10.1177/15593258221088709

Baltasar Sánchez, A., & González Sistal, Á. (2014). A quantitative method for the characterization of lytic metastases of the bone from

radiographic images. *The Scientific World Journal*, *2014*(1), Article 264836. https://doi.org/10.1155/2014/264836

Changsan, N., Atipairin, A., Sakdiset, P., Muenraya, P., Balekar, N., Srichana, T., Sritharadol, R., Phanapithakkun, S., & Sawatdee, S. (2024). BrSPR-20-P1 peptide isolated from *Brevibacillus* sp. developed into liposomal hydrogel as a potential topical antimicrobial agent. *RSC Advances, 14*(42), 27394–27411. https://doi.org/10.1039/D4RA03722G

Dangsaart, B., Boonyarattanakalin, K., Bangbai, C., Sungthong, A., & Chongsri, K. (2024). Enhanced optical and photocatalytic properties of Ag NPs decorated-ZnO composites. *Thai Journal of Nanoscience and Nanotechnology*, *9*(2), 1-10.

Dubey, S. P., Lahtinen, M., Särkkä, H., & Sillanpää, M. (2010). Bioprospective of Sorbus aucuparia leaf extract in development of silver and gold nanocolloids. *Colloids and Surfaces B: Biointerfaces*, *80*(1), 26-33. https://doi.org/10.1016/j.colsurfb.2010.05.024

Elmegdar, S., Elkheloui, R., Laktib, A., Mimouni, R., & Hamadi, F. (2024). Antibiofilm and anti-quorum sensing activities of biological nanoparticles. *Current Applied Science and Technology*, *24*(2), e0257479-e0257479. https://doi.org/10.55003/cast.2023.257479

Elumalai, A., & Navabshan, I. (2024). Fabrication of silver nanoparticles using acalypha paniculata extract, AI-based interaction analysis and its activity explication. *Natural and Life Sciences Communications*, *23*(3), Article e2024035. https://doi.org/10.12982/NLSC.2024.035

Fu, Y. H., Kuznetsov, A. I., Miroshnichenko, A. E., Yu, Y. F., & Luk'yanchuk, B. (2013). Directional visible light scattering by silicon nanoparticles. *Nature Communications*, *4*(1), Article 1527. https://doi.org/10.1038/ncomms2538

Irwan, I., Zulfahmi, I., & Nurliza, E. (2024). Green synthesis of silver nanoparticles using ulva intestinalis with cytotoxic and antioxidant activity. *Science & Technology Asia*, *29*(3), 315-325.

Kelly, K. L., Coronado, E., Zhao, L. L., & Schatz, G. C. (2003). The optical properties of metal nanoparticles: the influence of size, shape, and dielectric environment. *The Journal of Physical Chemistry B*, *107*(3), 668-677. https://doi.org/10.1021/jp026731y

Krishnaraj, C., Jagan, E. G., Rajasekar, S., Selvakumar, P., Kalaichelvan, P. T., & Mohan, N. (2010). Synthesis of silver nanoparticles using *Acalypha indica* leaf extracts and its antibacterial activity against water borne pathogens. *Colloids and Surfaces B: Biointerfaces, 76*(1), 50–56. https://doi.org/10.1016/j.colsurfb.2009.10.008

Lee, K. J., Park, S. H., Govarthanan, M., Hwang, P. H., Seo, Y. S., Cho, M., ... & Oh, B. T. (2013). Synthesis of silver nanoparticles using cow milk and their antifungal activity against phytopathogens. *Materials Letters*, *105*, 128-131. https://doi.org/10.1016/j.matlet.2013.04.076

Li, B., Chua, S. L., Yu, D., Chan, S. H., & Li, A. (2022). Detection, identification and size distribution of silver nanoparticles (AgNPs) in milk and migration study for breast milk storage bags. *Molecules*, *27*(8), Article 2539. https://doi.org/10.3390/molecules27082539

Maneewattanapinyo, P., Pichayakorn, W., Monton, C., Dangmanee, N., Wunnakup, T., & Suksaeree, J. (2023). Effect of ionic liquid on silver-nanoparticle-complexed Ganoderma applanatum and its topical film formulation. *Pharmaceutics*, *15*(4), Article 1098. https://doi.org/10.3390/pharmaceutics15041098

Martin, M. M., & Sumayao Jr, R. E. (2022). Facile green synthesis of silver nanoparticles using Rubus Rosifolius Linn aqueous fruit extracts and its characterization. *Applied Science and Engineering Progress*, *15*(3), 5511-5511. https://doi.org/10.14416/j.asep.2021.10.011

Pandey, S., De Klerk, C., Kim, J., Kang, M., & Fosso-Kankeu, E. (2020). Eco friendly approach for synthesis, characterization and biological activities of milk protein stabilized silver nanoparticles. *Polymers*, *12*(6), Article 1418. https://doi.org/10.3390/polym12061418

Rechberger, W., Hohenau, A., Leitner, A., Krenn, J. R., Lamprecht, B., & Aussenegg, F. R. (2003). Optical properties of two interacting gold nanoparticles. *Optics communications*, *220*(1-3), 137-141. https://doi.org/10.1016/S0030-4018(03)01357-9

Simatupang, C., Jindal, V. K., & Jindal, R. (2021). Biosynthesis of silver nanoparticles using orange peel extract for application in catalytic degradation of methylene blue dye. *Environment and Natural Resources Journal*,

19(6), 468-480. https://doi.org/10.32526/ennrj/19/202100088

Subavathy, P., & Grace, G. A. J. (2023). Biogenic synthesis, characterization and applications of Tellurium nanoparticles from Chicoreus virgineus (Roding, 1798). *Journal of Current Science and Technology*, *13*(2), 237-250. https://doi.org/10.59796/jcst.V13N2.2023.1742

Sukmongkolwongs, C., Sawasiticher, P., & Wutticharoenmongkol, P. (2024). Electrospun cellulose acetate nanofibers containing *Clinacanthus nutans* (Phayayo) crude extract as potential wound dressings. *Journal of Current Science and Technology, 14*(1), Article 7. https://doi.org/10.59796/jcst.V14N1.2024.7

Suknicom, S., & Borompichaichartkul, C. (2021). Stability and phase behavior of fish oil emulsion containing konjac glucomannan in goat milk systems. *Journal of Current Science and Technology*, *11*(3), 392-401. https://doi.org/10.14456/jcst.2021.39

Thamilselvi, V., & Radha, K. V. (2017). Silver nanoparticle loaded silica adsorbent for wastewater treatment. *Korean Journal of Chemical Engineering*, *34*(6), 1801-1812. https://doi.org/10.1007/s11814-017-0075-4

Thongwattana, T., Chaiyo, R., Ponsanti, K., Tangnorawich, B., Pratumpong, P., Toommee, S., ... & Pechyen, C. (2024). Synthesis of silver nanoparticles and gold nanoparticles used as biosensors for the detection of human serum albumin-diagnosed kidney disease. *Pharmaceuticals*, *17*(11), Article 1421. https://doi.org/10.3390/ph17111421